JACS
JOURNAL OF THE AMERICAN CHEMICAL SOCIETY
Article
pubs.acs.org/JACS

Galvanic Replacement of the Liquid Metal Galinstan

Faegheh Hoshyargar, Jessica Crawford, and Anthony P. O'Mullane*

†School of Chemistry, Physics and Mechanical Engineering, Queensland University of Technology (QUT), Brisbane, QLD 4001, Australia

Supporting Information

ABSTRACT: The galvanic replacement reaction is a highly versatile approach for the creation of a variety of nanostructured materials. However, the majority of reports are limited to the replacement of metallic nanoparticles or metal surfaces. Here we extend this elegant approach and describe the galvanic replacement of the liquid metal alloy galinstan with Ag and Au. This is achieved at a macrosized droplet to create a liquid metal marble that comprises a liquid metal core and a solid metal shell, whereby the morphology of the outer shell is determined by the concentration of metallic ions used in the solution during the galvanic replacement process. In principle, this allows one to recover precious metal ions from solution in their metallic form, which are immobilized on the liquid metal and therefore easy to recover. The reaction is also undertaken at liquid metal microdroplets created via sonication to produce Ag- and Au-based galinstan nanorice particles. These materials are characterized with SEM, XRD, TEM, SAED, EDX, XPS, UV−visible spectroscopy, and open-circuit potential versus time experiments to understand the galvanic replacement process. Finally, the nanosized materials are investigated for their catalytic activity toward the reduction of methylene blue in the presence of sodium borohydride. This approach illustrates a new avenue of research for the galvanic replacement process and, in principle, could be applied to many more systems.

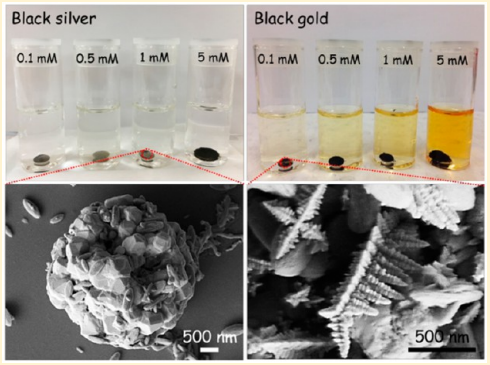

INTRODUCTION

Galvanic replacement involving nanoscale objects has been the subject of intensive research since 2002, when it was first reported by Xia and colleagues.[1] Since then, several comprehensive review articles have been written on the subject either directly or as part of a broader review of hollow and porous materials.[2−10] Although the electrochemical principle behind this reaction is considerably older, Xia was the first to demonstrate the phenomenon on the nanoscale, where hollow Au nanostructures were created from Ag nanoparticles.[1] The electrochemical reaction is straightforward in that a sacrificial template, such as Ag, is oxidized in the presence of ions of a different metal, such as Au^{3+}, which have a higher reduction potential and thus are subsequently reduced to the metallic state at the template surface. Under appropriate reaction conditions, a variety of nanostructured materials can be formed, such as hollow nanoparticles of different shapes, sizes, and compositions. This can be extended further by combination with a co-reduction reaction, whereby a reductant can be introduced to create bimetallic or alloyed hollow nanostructures or layered nanomaterials.[2] With regard to the galvanic replacement of metallic nanoparticles and macroscopic surfaces, the field is very mature, and the resultant materials have been used in numerous (electro)catalytic, plasmonic, and biomedical imaging applications.[11−18]

There have also been reports to extend the concept of galvanic replacement to systems other than pure metals. Oh et al. have demonstrated that Mn_3O_4 nanocrystals could be galvanically replaced using iron perchlorate to produce hollow nanocrystals of Mn_3O_4/γ-Fe_2O_3, which ultimately converted into cagelike γ-Fe_2O_3 nanomaterials.[19] These were utilized as anode materials in Li ion batteries. Metal oxides such as Cu_2O have also been galvanically replaced in solutions of appropriate pH to create Cu_2O/Pd and Cu_2O/Au nanocomposites.[20] Other reports have included the galvanic replacement of semiconducting organic charge-transfer complexes such as MTCNQ (TCNQ = tetracyanoquinodimethane) and $MTCNQF_4$ ($TCNQF_4$ = 2,3,5,6-tetrafluoro-7,7,8,8-tetracyanoquinodimethane) with Au, Ag, Pt, and Pd nanomaterials for (photo)catalytic applications.[21−24]

Therefore, it is clear that the process of galvanic replacement is attractive because excellent control can be achieved on the nanoscale and can be tuned for the application of interest. However, to date, there has not been an attempt to explore the galvanic replacement of a liquid metal such as galinstan, which is a room-temperature liquid metal alloy of 68.5% gallium, 21.5% indium, and 10.0% tin. It is apparent that the individual metal components can be readily oxidized when the electrochemical series is considered, and oxidants such as Ag^+ and Au^{3+} ions should facilitate the galvanic replacement process. It is noteworthy that liquid metals in their own right have received significant attention recently in such diverse areas as plasmonics,[25,26] liquid metal enabled pumps,[27] actuators,[28]

Received: June 10, 2016
Published: September 14, 2016

DOI: 10.1021/jacs.6b05957
J. Am. Chem. Soc. 2017, 139, 1464−1471

coolants,[29] electronics,[30,31] fluidic antennas,[32] wearable sensors,[33,34] repairable circuitry,[35] and microfluidics[36] and also when modified into liquid metal marbles consisting of a coating of semiconducting nanomaterials on the liquid metal core.[37] The latter has been used in photocatalytic applications, electrochemical heavy metal ion sensing, and actuator applications.[37−39] Therefore, liquid metals are not only a system of fundamental interest; the ability to manipulate the chemistry of liquid metals in a facile manner may have significant implications for many applications as well.

In this work we explore the galvanic replacement of liquid metal galinstan with Ag and Au both on the bulk scale to generate liquid metal core/solid metal shell marbles and on the nanoscale to form nanorice particles. We explore the latter as heterogeneous catalysts for the degradation of the dye methylene blue in the presence of sodium borohydride. We believe this approach opens up a new avenue of research in the important area of galvanic replacement.

EXPERIMENTAL SECTION

Materials and Chemicals. Potassium tetrabromoaurate(III) hydrate ($KAuBr_4{\cdot}xH_2O$, 99.9%), potassium gold(III) chloride ($KAuCl_4$, 99.995%), polyvinylpyrrolidone (PVP, average molar weight = 10 000), and sodium borohydride ($NaBH_4$, 99.99%) were purchased from Sigma-Aldrich. Methylene blue (MB) was obtained from EMD Chemicals and silver nitrate ($AgNO_3$, 95%) from Australian Chemical Reagents. Galinstan (galinstan fluid 4 N) was purchased from Geratherm Medical AG.

Galvanic Replacement Process. In the initial experiments, a galinstan droplet was placed in aqueous solutions of $AgNO_3$ or $KAuBr_4$ of different concentrations ranging from 0.1 to 5 mM, or in 0.1 or 1 mM aqueous solution of $KAuCl_4$, for 72 h. For the galvanic replacement of microsized galinstan, a liquid droplet was sonicated in an aqueous solution of either $AgNO_3$ or $KAuBr_4$. The Ag-GaInSn material was prepared by sonicating 80 mg of galinstan in 4.9 mL of aqueous solution of 5 mM $AgNO_3$ for 30 min, followed by adding 0.1 mL of aqueous solution of 5 mg/mL PVP to the solution. The Au-GaInSn material was prepared by sonicating 200 mg of galinstan in 5 mL of aqueous solution of 1 mM $KAuBr_4{\cdot}xH_2O$ for 30 min. All aqueous solutions were prepared from water (resistivity of 18.2 MΩ·cm at 25 °C) purified by use of a Milli-Q reagent deionizer (Millipore). Sonication was carried out in a sonication bath (Soniclean Pty. Ltd. Soniclean 750HT, 220/240 V AC, 50/60 Hz, 380 W).

Material Characterization. Material characterization was carried out using field emission scanning electron microscopy (FESEM, Zeiss Sigma VP field emission scanning electron microscope equipped with an Oxford XMax 50 Silicon Drift energy-dispersive X-ray detector at 20 kV under high-vacuum), high-resolution transmission electron microscopy and selected area electron diffraction (HRTEM and SAED, JEOL 2100 200 kV transmission electron microscope equipped with high-sensitivity silicon drift X-ray detector (Oxford XMax) for compositional analysis, with an ultra-high-resolution pole piece, Gatan Orius SC1000 CCD camera and LaB_6 gun), X-ray photoelectron spectroscopy (XPS, Omicron MultiProbe system using a non-monochromated Al Kα X-ray source), and UV−visible spectroscopy (Agilent Cary 60 UV−visible spectrophotometers). Colloidal nanocomposites were drop-cast onto cleaned Si wafers and amorphous carbon-coated copper grids for SEM and TEM studies, respectively, and immobilized by solvent evaporation. SEM samples of the large droplets of galinstan modified with silver or gold were prepared by collecting the skin formed on the galinstan droplet, dispersing in deionized water (DIW), and drop-casting onto cleaned Si wafers. A colloidal solution of Ag-GaInSn was diluted five times to prepare samples for SEM, TEM, and UV−vis absorption studies. The XPS data were analyzed using CasaXPS software version 2.3.16. Two dimensional (2D) X-ray diffraction (XRD) patterns were acquired with a Rigaku SmartLab using a copper target (40 kV, 40 mA) and a Hypix 3000 detector (vertical orientation). A parallel beam was generated by the cross beam optics unit and then further conditioned to a smaller area using a CBO-*f* unit and 0.5 mm height-limiting slit. The samples were placed on a stage that allows for movement in the X and Y directions. A flat part of the sample was chosen for analysis, and then 2D exposures (10 s) were collected across the 15−90° 2θ range. The exposures were then integrated to 0/1D profiles using Rigaku 2D Data Processing Software (2DP).

Electrochemical Experiment. A hanging galinstan drop electrode (HGDE) was used as the working electrode.[37] The reference electrode was Ag/AgCl (aqueous 3 M KCl), and platinum was used as the counter electrode. The electrochemical experiment was carried out using a Biologic VSP-300 potentiostat. A galinstan droplet suspended from a syringe was allowed to make contact with water immediately before running the open-circuit potential (OCP) versus time experiment. The required volume of $AgNO_3$ aqueous solution was injected into the cell to give a final concentration of 5 mM.

Catalytic Reaction. First, 0.1 mL of the catalyst (either colloidal Ag-GaInSn or Au-GaInSn) was injected into the reaction mixture with a total volume of 3 mL (containing 7.2×10^{-5} M MB and 1.2×10^{-2} M $NaBH_4$) in a quartz cuvette at (25 ± 2) °C, and the catalytic activity was monitored by UV−vis spectroscopy using an Agilent Cary 60 UV−visible spectrophotometer. For the control experiment, 80 mg of galinstan was sonicated in 5 mL of DIW for 30 min and used as the catalyst following the same procedure described for Ag-GaInSn and Au-GaInSn.

RESULTS AND DISCUSSION

Initial investigations were undertaken with a galinstan droplet placed in an aqueous solution of $AgNO_3$. The liquid metal droplets were exposed to 0.1, 0.5, 1, and 5 mM $AgNO_3$ aqueous solutions, and the changes in the appearance of the droplet were monitored and recorded at 24 h intervals up to 72 h. Figure 1 shows digital images which illustrate the significant

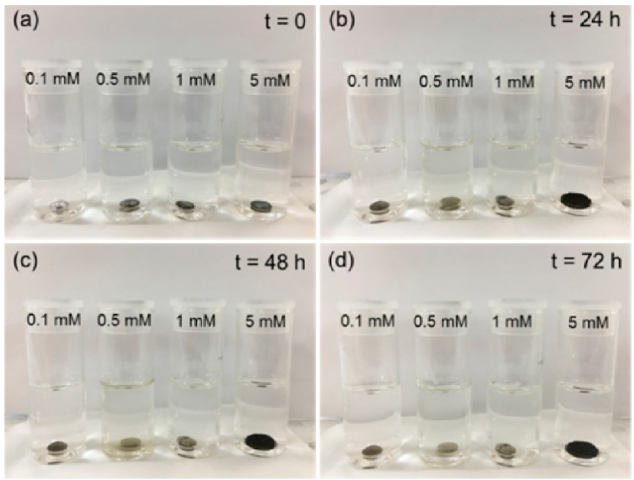

Figure 1. Formation of black silver on galinstan in $AgNO_3$ aqueous solutions of varied concentrations after (a) 0, (b) 24, (c) 48, and (d) 72 h.

changes in the appearance and morphology of the droplet as a function of concentration and time. Upon initial contact (t = 0) with the $AgNO_3$ solution, the shiny metallic galinstan droplets turned a gray color almost immediately, in particular in the case of higher concentrations, whereas the droplet in 0.1 mM remained pristine. However, after 24 h, a gray-colored skin formed on the galinstan droplet at the lowest concentration of 0.1 mM (Figure 1b). Interestingly, at t = 24 h, the galinstan droplet in the 5 mM $AgNO_3$ solution grew much larger than

DOI: 10.1021/jacs.6b05957
J. Am. Chem. Soc. 2017, 139, 1464−1471

the original droplet and turned black. The color of the outer coating did not change from t = 24 h to t = 48 h, while its thickness increased (Figure 1c,d). The outer black layers were allowed to develop for 72 h and were subsequently collected and subjected to further characterization by FESEM/EDX.

Figure 2a,b shows the FESEM images of the skin created in 0.1 mM solution after 72 h. At this very low concentration, the

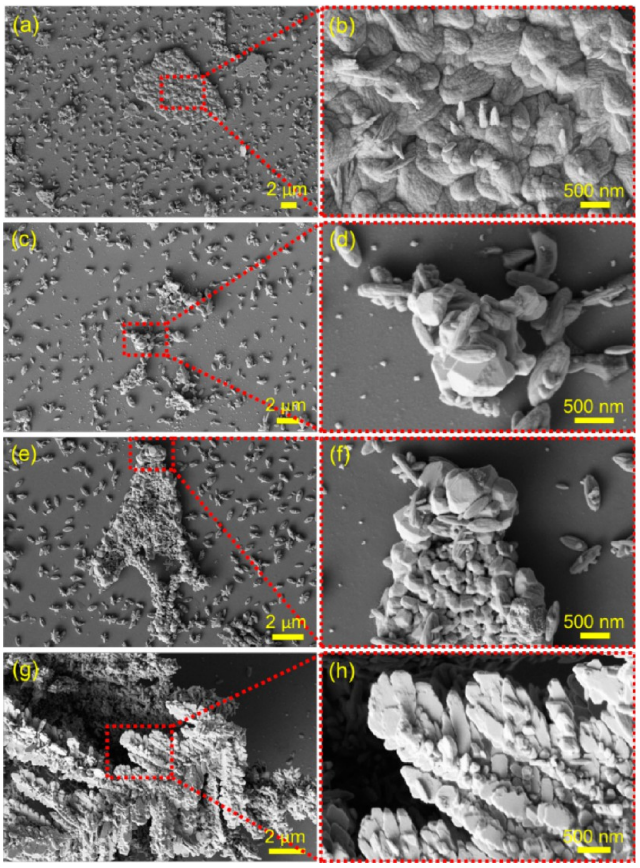

Figure 2. FESEM images of black silver formed on a galinstan droplet in (a,b) 0.1, (c,d) 0.5, (e,f) 1, and (g,h) 5 mM $AgNO_3$ aqueous solution.

outer skin that is formed is very thin and consists of structures that are consistent with oxidized galinstan, i.e., wrinkled microstructures that are indicative of Ga_2O_3.[38] There is some evidence of small, spherical-shaped particles (Figure 2b), attributed to the formation of metallic silver (EDX analysis shows a 2.9% Ag content, Table S1). The morphology of the outer skin changed considerably at the higher $AgNO_3$ concentrations of 0.5 mM (Figure 2c,d) and 1 mM (Figure 2e,f). Here more block-like crystals were formed, and the Ag content increased to 10.7% and 11.2%, respectively (Table S1). The outer skin obtained from the 5 mM $AgNO_3$ solution also showed a marked difference in morphology from the other samples and is composed of micrometer-sized multipods which grow all over the skin. These multipods are geometrically asymmetric, and the branches grow in random directions, as shown in Figure 2g,h. The silver content in this case was significant and increased to 51.4% (Table S1).

The observations described here, including the formation of metallic Ag on the surface of the galinstan drop, indicate that a galvanic replacement process is occurring. In principle, galvanic replacement takes place at the liquid metal-solution interface, namely, the galinstan droplet's surface which serves as the sacrificial template for the growth of the obtained nanostructures. When the standard reduction potentials of Ga^{3+}/Ga^0, In^{3+}/In^0, Sn^{2+}/Sn^0, and Ag^+/Ag^0 (−0.529, −0.340, −0.138, and 0.799 V vs SHE,[40] respectively) are considered, it indicates that there are significant thermodynamic driving forces for such a replacement reaction to take place. This will occur in an analogous manner to that seen for the many reports in the literature that describe this phenomenon. The major difference in this case is that the template is a liquid rather than a solid nanoparticle or surface as reported previously. For the case of galinstan, in principle all three components of the liquid can be replaced when in contact with $AgNO_3$ with the highest driving force being for the replacement of Ga, which has the lowest standard reduction potential. This is reflected in the EDX data where the consumption of Ga is the most rapid when increasing the $AgNO_3$ concentration (Table S1). This redox reaction between Ga and Ag^+ ions can be represented by eq 1.

$$Ga^0 + 3Ag^+ \rightarrow Ga^{3+} + 3Ag^0 \quad (1)$$

Upon liberation, Ga^{3+} ions will immediately react with dissolved O_2 to form Ga_2O_3, which accounts for the large concentration of oxygen found in the EDX analysis. Therefore, the outer skin of galvanically replaced galinstan consists of Ga_2O_3, metallic Ag, and minor components of In and Sn.

In order to study whether the galvanic replacement of galinstan is possible with other metals, this experiment was also carried out using a gold salt. In this case, galinstan droplets were placed into aqueous solutions of $KAuBr_4$, and on this occasion changes in the color of the solution could be monitored as well as in the appearance of the liquid droplet. Similar to the silver case, a black skin was readily formed on galinstan at the initial point (t = 0) in the case of the 5 mM gold salt solution; however, this was not the case for solutions with lower concentrations (Figure 3a). As observed in Figure 3b, the development of a black skin on galinstan droplets in the lower concentration solutions was only initiated after 24 h. Again as the template, the galinstan's surface is where the black skin grows after the galvanic replacement of Ga/Sn/In elements with $AuBr_4^-$ ions. There is also a significant driving force for

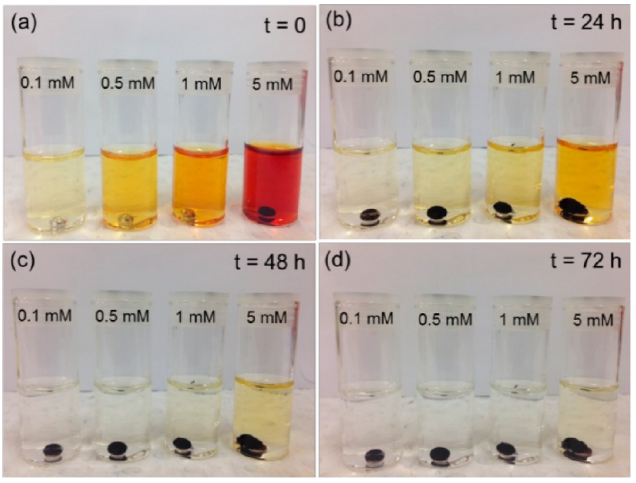

Figure 3. Formation of black gold on galinstan in $KAuBr_4$ aqueous solutions of varied concentrations after (a) 0, (b) 24, (c) 48, and (d) 72 h.

DOI: 10.1021/jacs.6b05957
J. Am. Chem. Soc. 2017, 139, 1464−1471

this reaction to occur when the standard reduction potential of the $AuBr_4^-/Au^0$ couple of 0.85 V vs SHE is considered.

From the EDX analysis (Table S2), the major reactant is Ga, and the reaction can be presented as

$$Ga^0 + AuBr_4^- \rightarrow Ga^{3+} + Au^0 + 4Br^- \quad (2)$$

Figure 3c,d indicates that the growth of this black skin continues with time and that the thickness of the outer skin increases until all the $AuBr_4^-$ ions in the solution are consumed (the solution becomes colorless). As can be seen from the images, compared to the fresh droplet, the galinstan becomes highly elongated with time, which is assumed to be due to the extra weight of material that is being added by the developing skin (best observed in the 5 mM solution as the skin is thicker and therefore heavier). After 72 h, the outer skins were subjected to further investigations by a combined FESEM/EDX analysis.

As illustrated in Figure 4a,b, at the lowest concentration of 0.1 mM, the growth of gold is limited (0.6% Au, see Table S2).

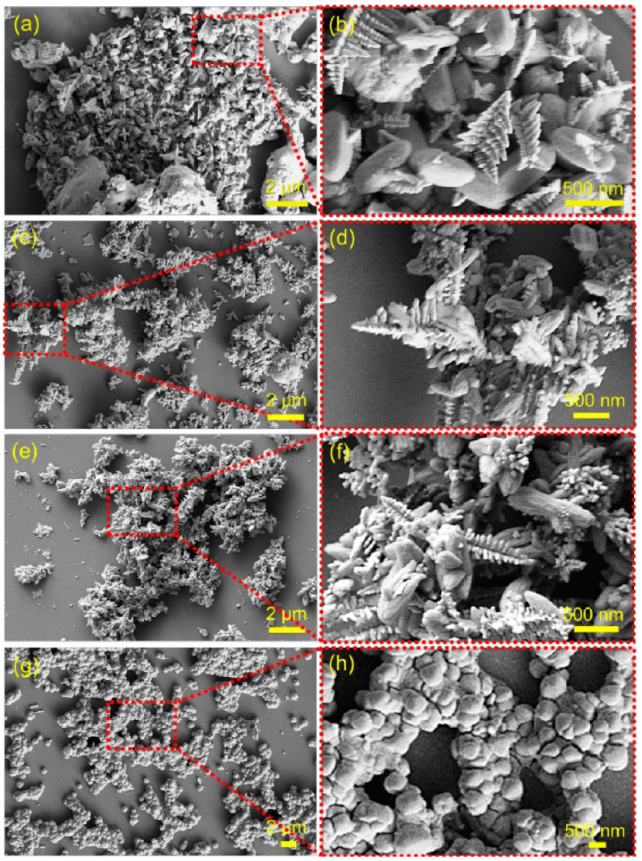

Figure 4. FESEM images of black gold formed on a galinstan droplet in (a,b) 0.1, (c,d) 0.5, (e,f) 1, and (g,h) 5 mM $KAuBr_4$ aqueous solution.

However, even at this low concentration, well-defined hierarchical nanostructures are formed which are composed of multipod assemblies of Au nanoparticles, which is significantly different from the silver case where spherical particles were formed (Figure 2b). The formation of dendritic materials in the case of gold can be attributed to the liberation of Br^- ions into solution (eq 2), where it is known from electrochemical studies that the presence of halides can promote the formation of anisotropic structures.[41,42] It is also known that Br^- ions interact strongly with specific crystal facets of gold which would perturb the growth process.[43] Interestingly, when the $KAuBr_4$ solution was replaced with a $KAuCl_4$ solution, elongated dendrites were not formed as shown in Figure S1a,b for 0.1 mM and in Figure S1c,d for 1 mM solution, confirming a strong interaction of the liberated bromide ions with the growing gold deposit rather than with chloride ions. At 0.5 mM, hierarchical structures were also formed but with fewer branches (Figure 4c,d), and the Au contribution increased quite substantially to 21.8% (Table S2). Figure 4e,f shows the morphology of the nanostructures obtained in a 1 mM $KAuBr_4$ solution, where branch formation becomes even more inhibited and the Au content increases to 47.3% (Table S2). At 5 mM $KAuBr_4$ (Figure 4g,h), no branched structures are formed; instead, large block-like crystals which are coalesced are evident. The gold content under these conditions increases to 55.6% (Table S2). At the higher $KAuBr_4$ concentrations the rate of reduction is significantly faster, and therefore the formation of branched dendritic like structures is suppressed, even in the presence of bromide ions. The formation of the dendrites is generally favored by slower growth conditions in dilute solutions where the diffusion limited aggregation growth model operates.[44] Under the conditions of high concentration, the growth process is too rapid to allow this to occur or be influenced by the presence of growth directing halide ions, and therefore denser and less open structures are formed. XRD experiments confirm that the silver and gold outer shells formed via galvanic replacement of galinstan in low and high concentration metal salt solutions are polycrystalline with a face-centered cubic crystal structure (Figure 5). This was also

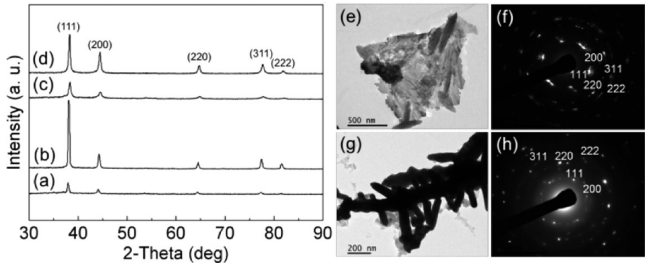

Figure 5. XRD patterns of black silver and black gold formed on a galinsten droplet in (a) 0.5 and (b) 5 mM $AgNO_3$ and (c) 0.5 and (d) 5 mM $KAuBr_4$ aqueous solutions. TEM (left) and SAED patterns (right) of black silver (top) and black gold (bottom) formed on galinstan droplets in (e,f) 5 mM $AgNO_3$ and (g,h) 5 mM $KAuBr_4$ aqueous solutions.

confirmed by SAED experiments (Figure 5f,h), which show the polycrystalline nature of both the Ag and Au samples. There are also no peaks present for Ga_2O_3, indicating that the surface oxide is amorphous.

As previously mentioned, the galvanic replacement reaction takes place at the galinstan-solution interface. At the concentration of metal salts used here, complete consumption of the liquid metal is unlikely to occur, and the metal salts are the limiting reagents, as evidenced by the almost complete disappearance of the characteristic red/orange color of $KAuBr_4$ after 72 h. To illustrate this, the galvanically replaced liquid metal drop was removed from the solution and cut with a scalpel blade, which shows the shiny unreacted liquid metal core as well as the outer skin (Figure 6 and Video S1). This confirms that, under these conditions, a liquid metal marble is

DOI: 10.1021/jacs.6b05957
J. Am. Chem. Soc. 2017, 139, 1464−1471

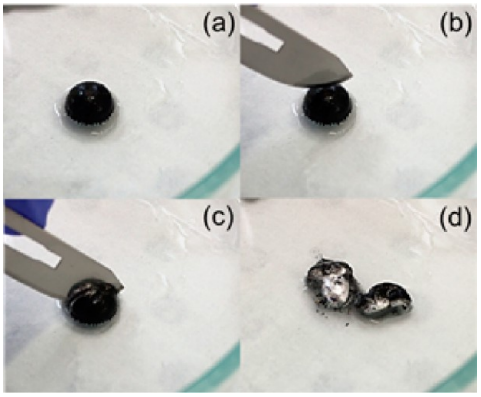

Figure 6. Successive snapshots of cutting through the black gold skin, exposing unreacted galinstan in the core.

formed that consists of a solid metal shell encapsulating a liquid metal core. EDX analysis of the core of this marble indicates that its composition is unchanged from the starting material (Figure S2).

This system is quite different from those observed in previous studies on liquid metal marbles,[37] where liquid galinstan was modified with powders of semiconducting material such as WO_3, and this approach may open up a new avenue of research into these interesting liquid metal marble systems. It also indicates a possible route for the recovery of precious metals that are in their ionic form. In principle, any metal ion that has a standard reduction potential higher than that of Ga^0/Ga^{3+} could be recovered in an aqueous solution. We also investigated the reduction of Pd^{2+}, Pt^{2+}, and Cu^{2+} ions and found that metal shells are also created on the galinstan droplet in each case. For the case of copper the reaction was found to be much slower than all other systems (1 week to form a non-continuous film on a galinstan drop) and can be related to the less positive standard reduction potential of the Cu^{2+}/Cu^0 (0.340 V vs SHE) couple compared to that of the Ag, Au, Pt, and Pd systems. This indicates that the major driving force is likely to be thermodynamic in nature and not dictated by the number of electrons involved in the replacement process.

From previous studies on liquid metal gallium−indium[45] and galinstan, it was found that sonicating liquid metals in solution resulted in the formation of liquid metal micro-/nanodroplets that improved the performance in particular for galinstan in applications such as heavy metal ion sensing,[38] gas sensing,[46] photocatalysis,[39] and heterogeneous catalysis.[47] Therefore, the galvanic replacement of galinstan was also studied under sonication conditions. For this experiment a galinstan droplet was sonicated in 5 mM $AgNO_3$ aqueous solution for 30 min. Under sonication, the liquid metal breaks apart into smaller particles, which, in principle, should increase the reactivity toward silver ions due to a simple increase in surface area of the liquid metal. It was found that the solution turned yellow only a few seconds after sonication, which is highly indicative of the formation of Ag nanostructured materials. The reaction was carried out for 30 min after which 0.1 mL of PVP aqueous solution (5 mg/mL), a known nanoparticle capping agent,[48] was added to the solution to maintain the stability of obtained nanocomposite in colloidal form (final concentration of PVP was 0.1 mg/mL). When PVP was not added, the particles agglomerated while the addition of the stabilizing agent increased the lifetime of the colloidal suspension up to 7 days. The material formed with this approach is denoted as Ag-GaInSn.

Figure 7a shows an overview FESEM image of the as-synthesized Ag-GaInSn. As observed in Figure 7b, the product

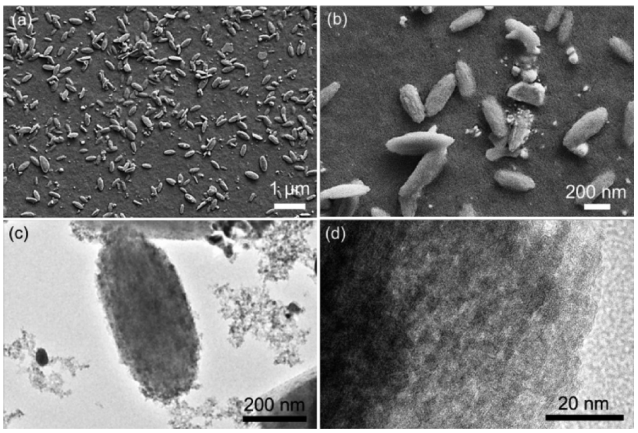

Figure 7. FESEM and TEM images of Ag-GaInSn nanocomposite. (a) Overview and (b) magnified FESEM image, (c) correspondent TEM image, and (d) HRTEM image of an individual nanorice particle.

is composed of monodispersed nanorice-like particles with dimensions of on average 500 nm × 150 nm. A HRTEM image is shown in Figure 7c. The nanorice particles are, in fact, composed of smaller particles assembled to form ellipsoid grains (Figure 7d). EDX analysis of Ag-GaInSn nanocomposite (Table S3) revealed a contribution of 4.5% silver in the nanocomposite (sample diluted five times).

The formation of metallic Ag nanoparticles was also confirmed by the appearance of a characteristic surface plasmon resonance (SPR) band at 438 nm as monitored by UV−vis spectroscopy (Figure 8a). Some distinct spherical particles can

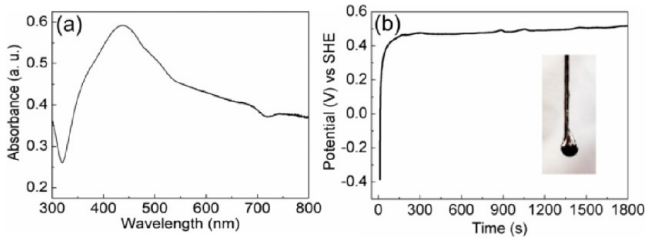

Figure 8. (a) UV−vis spectrum of Ag-GaInSn nanocomposite solution. (b) OCP vs time recorded in 5 mM $AgNO_3$ solution with HGDE as a working electrode (inset: HGDE half-submerged in the electrolyte solution in OCP experiment).

also be observed in the SEM images in Figure 7a,b that are not part of the nanorice particles which are responsible for the observation of the well-defined SPR peak at 438 nm. The broad absorption from 450 to 700 nm could be attributed to the nanorice particles. The hypothesis that Ag nanoparticles are formed as a result of galvanic replacement reaction was also confirmed electrochemically. A HGDE was immersed into a 5 mM $AgNO_3$ solution, and an OCP versus time experiment was carried out (Figure 8b). The experiment was run for 30 min for consistency with the sonication time. The experiment was carried out by injecting $AgNO_3$ into water where the HGDE was already in position to capture the first contact of galinstan with Ag^+ ions. The rapid rise of potential from −0.39 to 0.46 V

DOI: 10.1021/jacs.6b05957
J. Am. Chem. Soc. 2017, 139, 1464−1471

within the first 160 s indicates that galinstan rapidly oxidizes in the presence of Ag^+ ions. After 160 s, the potential continues to increase but at a very slow rate and does not reach the expected value for an Ag electrode in 5 mM $AgNO_3$ of 0.663 V vs SHE. This is due to the surface not being entirely composed of silver as there is also Ga_2O_3 present as well as the consumption of Ag^+ ions which will affect the potential of the electrode. After the experiment it can be seen from the inset in Figure 8b that the part of the HGDE that was immersed into the electrolyte is covered with the black silver skin as seen in Figure 1.

The galvanic replacement of galinstan with gold was also studied using the sonication approach. When galinstan was sonicated in a 1 mM aqueous solution of $KAuBr_4$ for 30 min a pink color formed which is highly indicative of gold nanoparticle formation. The as-obtained particles were then investigated by FESEM and HRTEM (Figure 9). Nanorice

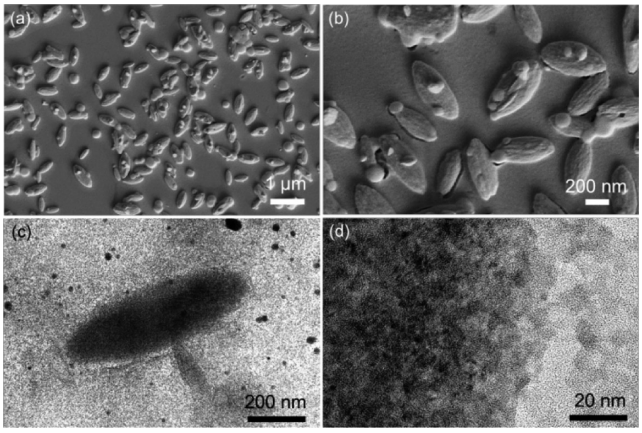

Figure 9. FESEM and TEM images of Au-GaInSn nanocomposite. (a) Overview and (b) magnified FESEM image, (c) correspondent TEM, and (d) HRTEM image of an individual nanorice particle.

particles were also observed which are quite similar to those formed when $AgNO_3$ was used (Figure 7); however, they are slightly larger (600 nm × 250 nm). Similar to the Ag analogue, the nanorice particles appear to be porous and made up of smaller particles (Figure 9d). EDX analysis (Table S3) revealed a 5.2% contribution of Au nanoparticles.

EDX mapping (Figure 10) and an EDX profile (Figure S3) clearly show the presence of Ga, In, Sn, Au, and O elements. However, the In content in the nanorice particles is particularly depleted when compared to starting galinstan (which could be observed from the In line in Figure S3). This is most likely due to the formation of the stable $KInBr_3$ species during the course of the galvanic replacement of metallic In with gold ions (Figure S4). From the EDX mapping data, it is apparent that there is some gold contained within the nanorice particles. There is a significant amount of gold that surrounds the nanorice particles but which also is present as isolated nanoparticles (Figure 10).

It is not surprising that isolated nanoparticles of both Ag and Au are formed with this approach, as under sonication conditions any metallic nanoparticle that is formed under these forces could detach from the liquid metal. For the large droplet (Figures 1 and 3), the reaction occurs under quiescent conditions, and therefore Ag and Au can nucleate and grow into solution and not detach from the liquid droplet. It is notable that the colloidal nanocomposite was stable in the solution even after 30 days without the need for a stabilizing

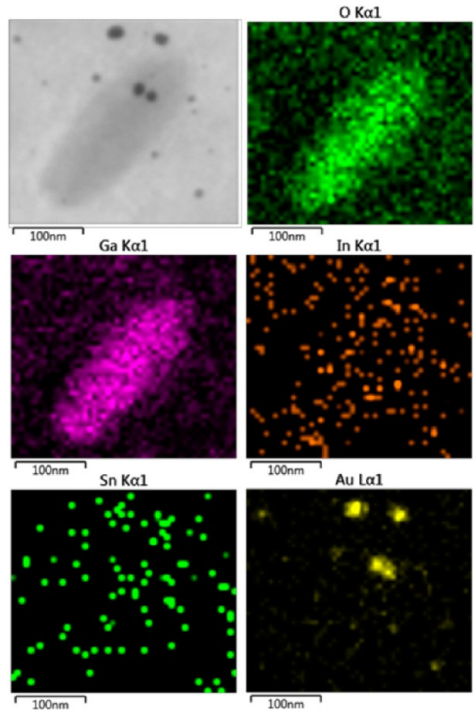

Figure 10. EDX mapping of Au-GaInSn nanocomposite obtained in 1 mM $KAuBr_4$ aqueous solution.

agent even when $KAuBr_4$ solution was added to galinstan after it had been previously sonicated (Figure S5). The formation of metallic gold is also readily observed by the appearance of a SPR band at 533 nm (Figure 11) and is due to the isolated Au nanoparticles formed during the reaction as seen in the TEM image in Figure 10.

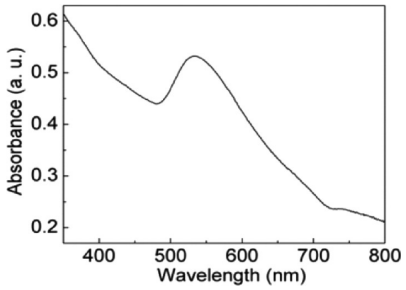

Figure 11. UV−vis spectrum of Au-GaInSn nanocomposite solution.

The surface composition of the Au-GaInSn was investigated in more detail using XPS. The Ga 3d core-level spectrum (Figure 12a), with a peak at 20.3 eV, consists of three components at 20.4, 18.6, and 15.9 eV, the latter being an overlapping In 4d (metallic indium) peak.[38] The In 3d core level spectrum shows two distinctive peaks at 445.3 and 452.9 eV (Figure 12b). These peaks are consistent of one major and one minor component, as shown in Figure 12b. The minor components at 443.2 (In $3d_{5/2}$) and 450.8 eV (In $3d_{3/2}$) are essentially contributed by In^0, whereas the major components at 445.4 and 452.9 eV reveal the formation of indium oxide (In_2O_3).[38] The Sn 3d spectrum (Figure 12c), with main peaks at 486.7 and 492.1 eV, shows a comparable contribution of metallic tin and tin oxide (Sn^{4+}) on the surface.[38] Figure 12d shows the XPS spectrum of the O 1s core level spectrum where

DOI: 10.1021/jacs.6b05957
J. Am. Chem. Soc. 2017, 139, 1464−1471

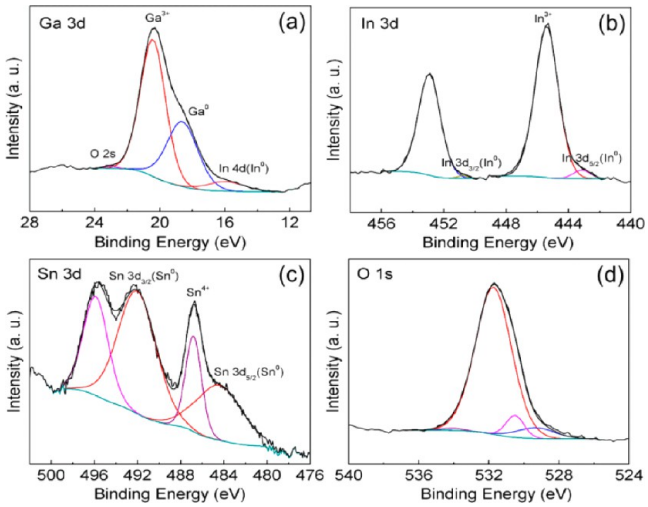

Figure 12. XPS spectra of Au-GaInSn nanocomposite. (a) Ga 3d, (b) In 3d, (c) Sn 3d, and (d) O 1s core-level spectra.

the peak fitting shows a major component at 531.7 eV corresponding to the formation of metal oxides accompanied by three minor components at 529.5, 530.5, and 534.1 eV, consistent with C−O and C═O species probably associated with organic contaminant loosely attached to the surface. These data are consistent with the galinstan surface being oxidized during the galvanic replacement process, thereby giving up electrons for the reduction of gold ions to metallic gold and primarily forming Ga_2O_3 with contributions from In_2O_3 and SnO_2 due to the oxygenated aqueous environment under which the reaction is undertaken.

Metallic nanoparticles are well known for their catalytic activity toward electron charge-transfer reactions. Recently we demonstrated the *in situ* formation of catalytically active materials from a galinstan precursor using $NaBH_4$.[47] In order to explore the applicability of the colloidal Ag-GaInSn and Au-GaInSn materials, we studied the degradation of MB using $NaBH_4$ in the presence of Ag- and Au-based nanocomposites. Therefore, colloidal solutions (0.1 mL) were added to MB and $NaBH_4$ solution mixtures in a cuvette, and the progress of the reaction was monitored by UV−vis spectroscopy. The reduction of MB to leucomethylene blue could be monitored by measuring the intensity of the characteristic band at 664 nm associated with the oxidized form (MB^+) that gives rise to an intense blue color in oxygenated environments.[49] As depicted in Figure 13a, in the case of Ag-GaInSn, the intensity of the peak at 664 nm was reduced by 80% in only 2 min. When Au-GaInSn was utilized, the intensity of the peak decreased by 63%

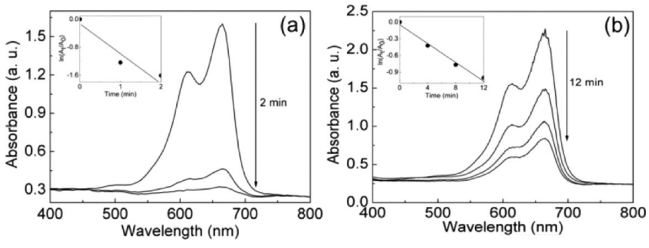

Figure 13. Time-dependent UV−vis absorption spectra of the reduction of 7.2×10^{-5} M MB by an excess of $NaBH_4$ in the presence of (a) Ag-GaInSn and (b) Au-GaInSn-based catalysts. Insets: plots of $\ln(A_t/A_0)$ versus time.

in 12 min (Figure 13b). Therefore, the Ag-GaInSn catalyst delivers better catalytic activity compared to Au-GaInSn, which is evident by the larger reaction rate (0.805 vs 0.084 min^{-1}). In a control experiment the catalysts were kept in 1.2×10^{-2} M $NaBH_4$ for 180 min and subsequently studied by SEM and EDX. In the case of the Ag-GaInSn-based catalyst, the morphology changed to micrometer-sized spherical particles decorated with Ag nanoparticles during the course of contact with the reducing media. The composition also changed where the gallium concentration was significantly reduced (to ∼3%), whereas the indium, tin, and silver elements were preserved, with indium and tin maintaining a 2:1 ratio (Figure S6). In fact, gallium was dissolved to produce sodium gallate ($NaGa(OH)_4$) as confirmed by EDX mapping (Figure S7). This is very similar to what we observed previously when galinstan was used as a catalyst for 4-nitrophenol reduction using $NaBH_4$.[47] In that case, when galinstan was brought into contact with $NaBH_4$, gallium leached out of the liquid metal leaving behind a catalytically active solid In/Sn rich spherical micro-/nanosized particles. Pure galinstan was also investigated for the MB reduction reaction, whereby a galinstan droplet sonicated in water was used as the catalyst. It was found that there was some catalytic activity (Figure S8), with a reaction rate of 0.011 min^{-1}, which is significantly lower than that observed with Ag or Au present. Therefore, the Ag and Au nanomaterials facilitate the two-electron-transfer process between BH_4^- and MB^+ and increase the electron capacity of the catalyst. This behavior is consistent with previous studies where Se nanowires decorated with Au nanoparticles showed increased activity for this reaction compared to only Se nanowires.[50] The observation in the current experiment confirms that, indeed, the enhanced catalytic activity of the material obtained from the Ag-based nanocomposite could be due to a synergistic contribution of Ag- and In/Sn-rich particles. In contrast, when the Au-GaInSn-based catalyst was treated with $NaBH_4$, the nanorice morphology was not compromised, and the Ga content was maintained in the sample (Figure S9). In addition, the presence of discrete Au nanoparticles could still be observed in the sample. In this system, it appears that the presence of Au rather than Ag stabilizes Ga in the nanorice particles against leaching in the $NaBH_4$ solution. This observation may also explain the lower catalytic activity of the Au-based catalyst as the presence of higher levels of gallium in galinstan-based materials impairs catalytic activity for these types of reactions.

■ CONCLUSION

In this work, we have demonstrated that the galvanic replacement of the liquid metal galinstan is possible via simple immersion in $AgNO_3$ or $KAuBr_4$ aqueous solutions. For large liquid metal droplets, the outer surface is converted into a solid Ag- or Au-rich material while the core remains liquid. The compositions and morphology of the outer metallic skin are determined by the precursor metal ion salt concentration. This process can be readily extended to other metals such as platinum, palladium, and copper and illustrates how precious metal ions can be easily recovered from aqueous solution. At the micro-/nanoscale, micrometer-sized droplets of galinstan created via sonication in the presence of $AgNO_3$ and $KAuBr_4$ resulted in the formation of Ag-GaInSn and Au-GaInSn nanorice particles as well as isolated Ag and Au nanoparticles. These materials were investigated for their catalytic activity for the reduction of methylene blue in the presence of $NaBH_4$, where it was found that the Ag-GaInSn material performed

DOI: 10.1021/jacs.6b05957
J. Am. Chem. Soc. 2017, 139, 1464−1471

better due to the conversion of the catalyst into a Ag-In/Sn-rich material. The work opens up a new approach to galvanic replacement and can be adopted to create many other combinations of liquid metal marbles or nanomaterials.

■ ASSOCIATED CONTENT

Supporting Information

The Supporting Information is available free of charge on the ACS Publications website at DOI: 10.1021/jacs.6b05957.

Tables S1−S3, summarizing EDX analyses; Figures S1−S9, showing FESEM images, EDX profiles, and time-dependent UV−vis absorption spectra (PDF)

Video S1, cutting through the black gold skin, exposing unreacted galinstan in the core (MPG)

■ AUTHOR INFORMATION

Corresponding Author

*anthony.omullane@qut.edu.au

Notes

The authors declare no competing financial interest.

■ ACKNOWLEDGMENTS

A.P.O. gratefully acknowledges support from the Australian Research Council (Future Fellowship FT110100760). The data reported in this paper were obtained at the Central Analytical Research Facility (CARF), operated by the Institute for Future Environments (QUT). Access to CARF is supported by generous funding from the Science and Engineering Faculty (QUT).

■ REFERENCES

(1) Sun, Y.; Mayers, B. T.; Xia, Y. *Nano Lett.* **2002**, *2*, 481.
(2) Xia, X.; Wang, Y.; Ruditskiy, A.; Xia, Y. *Adv. Mater.* **2013**, *25*, 6313.
(3) Cobley, C. M.; Xia, Y. *Mater. Sci. Eng., R* **2010**, *70*, 44.
(4) Wang, X.; Feng, J.; Bai, Y.; Zhang, Q.; Yin, Y. *Chem. Rev.* **2016**, DOI: 10.1021/acs.chemrev.5b00731.
(5) Zhu, C.; Du, D.; Eychmüller, A.; Lin, Y. *Chem. Rev.* **2015**, *115*, 8896.
(6) Jones, M. R.; Osberg, K. D.; Macfarlane, R. J.; Langille, M. R.; Mirkin, C. A. *Chem. Rev.* **2011**, *111*, 3736.
(7) Fang, Z.; Wang, Y.; Liu, C.; Chen, S.; Sang, W.; Wang, C.; Zeng, J. *Small* **2015**, *11*, 2593.
(8) Gilroy, K. D.; Farzinpour, P.; Sundar, A.; Hughes, R. A.; Neretina, S. *Chem. Mater.* **2014**, *26*, 3340.
(9) Niu, K.-Y.; Kulinich, S. A.; Yang, J.; Zhu, A. L.; Du, X.-W. *Chem. - Eur. J.* **2012**, *18*, 4234.
(10) Lu, X.; Chen, J.; Skrabalak, S. E.; Xia, Y. *Proc. Inst. Mech. Eng., Part N* **2007**, *221*, 1.
(11) Hu, S.; Tian, M.; Ribeiro, E. L.; Duscher, G.; Mukherjee, D. *J. Power Sources* **2016**, *306*, 413.
(12) Liu, D.; Li, W.; Feng, X.; Zhang, Y. *Chem. Science* **2015**, *6*, 7015.
(13) Jang, H.; Min, D.-H. *ACS Nano* **2015**, *9*, 2696.
(14) Qin, X.; Liu, L.; Xu, A.; Wang, L.; Tan, Y.; Chen, C.; Xie, Q. *J. Phys. Chem. C* **2016**, *120*, 2855.
(15) Sung, H. K.; Kim, Y. *Mater. Lett.* **2015**, *145*, 154.
(16) Yin, Y.; Erdonmez, C.; Aloni, S.; Alivisatos, A. P. *J. Am. Chem. Soc.* **2006**, *128*, 12671.
(17) Bansal, V.; Jani, H.; Du Plessis, J.; Coloe, P. J.; Bhargava, S. K. *Adv. Mater.* **2008**, *20*, 717.
(18) Chen, J.; Glaus, C.; Laforest, R.; Zhang, Q.; Yang, M.; Gidding, M.; Welch, M. J.; Xia, Y. *Small* **2010**, *6*, 811.
(19) Oh, M. H.; Yu, T.; Yu, S.-H.; Lim, B.; Ko, K.-T.; Willinger, M.-G.; Seo, D.-H.; Kim, B. H.; Cho, M. G.; Park, J.-H.; Kang, K.; Sung, Y.-E.; Pinna, N.; Hyeon, T. *Science* **2013**, *340*, 964.
(20) Susman, M. D.; Popovitz-Biro, R.; Vaskevich, A.; Rubinstein, I. *Small* **2015**, *11*, 3942.
(21) Pearson, A.; O'Mullane, A. P. *ChemPlusChem* **2013**, *78*, 1343.
(22) Pearson, A.; O'Mullane, A. P.; Bansal, V.; Bhargava, S. K. *Inorg. Chem.* **2011**, *50*, 1705.
(23) Pearson, A.; O'Mullane, A. P.; Bhargava, S. K.; Bansal, V. *Inorg. Chem.* **2012**, *51*, 8791.
(24) Pearson, A.; Ramanathan, R.; O'Mullane, A. P.; Bansal, V. *Adv. Funct. Mater.* **2014**, *24*, 7570.
(25) Blaber, M. G.; Engel, C. J.; Vivekchand, S. R. C.; Lubin, S. M.; Odom, T. W.; Schatz, G. C. *Nano Lett.* **2012**, *12*, 5275.
(26) Vivekchand, S. R. C.; Engel, C. J.; Lubin, S. M.; Blaber, M. G.; Zhou, W.; Suh, J. Y.; Schatz, G. C.; Odom, T. W. *Nano Lett.* **2012**, *12*, 4324.
(27) Tang, S.-Y.; Khoshmanesh, K.; Sivan, V.; Petersen, P.; O'Mullane, A. P.; Abbott, D.; Mitchell, A.; Kalantar-zadeh, K. *Proc. Natl. Acad. Sci. U. S. A.* **2014**, *111*, 3304.
(28) Sivan, V.; Tang, S.-Y.; O'Mullane, A. P.; Petersen, P.; Kalantar-zadeh, K.; Khoshmanesh, K.; Mitchell, A. *Appl. Phys. Lett.* **2014**, *105*, 121607.
(29) Hodes, M.; Zhang, R.; Lam, L. S.; Wilcoxon, R.; Lower, N. *IEEE Trans. Compon., Packag., Manuf. Technol.* **2014**, *4*, 46.
(30) So, J.-H.; Koo, H.-J.; Dickey, M. D.; Velev, O. D. *Adv. Funct. Mater.* **2012**, *22*, 625.
(31) Li, G.; Wu, X.; Lee, D.-W. *Sens. Actuators, B* **2015**, *221*, 1114.
(32) So, J.-H.; Thelen, J.; Qusba, A.; Hayes, G. J.; Lazzi, G.; Dickey, M. D. *Adv. Funct. Mater.* **2009**, *19*, 3632.
(33) Boley, J. W.; White, E. L.; Kramer, R. K. *Adv. Mater.* **2015**, *27*, 2355.
(34) Sheng, L.; Teo, S.; Liu, J. *J. Med. Biol. Eng.* **2016**, *36*, 265.
(35) Koo, H.-J.; So, J.-H.; Dickey, M. D.; Velev, O. D. *Adv. Mater.* **2011**, *23*, 3559.
(36) Dickey, M. D. *ACS Appl. Mater. Interfaces* **2014**, *6*, 18369.
(37) Sivan, V.; Tang, S.-Y.; O'Mullane, A. P.; Petersen, P.; Eshtiaghi, N.; Kalantar-zadeh, K.; Mitchell, A. *Adv. Funct. Mater.* **2013**, *23*, 144.
(38) Zhang, W.; Ou, J. Z.; Tang, S.-Y.; Sivan, V.; Yao, D. D.; Latham, K.; Khoshmanesh, K.; Mitchell, A.; O'Mullane, A. P.; Kalantar-zadeh, K. *Adv. Funct. Mater.* **2014**, *24*, 3799.
(39) Zhang, W.; Naidu, B. S.; Ou, J. Z.; O'Mullane, A. P.; Chrimes, A. F.; Carey, B. J.; Wang, Y.; Tang, S.-Y.; Sivan, V.; Mitchell, A.; Bhargava, S. K.; Kalantar-zadeh, K. *ACS Appl. Mater. Interfaces* **2015**, *7*, 1943.
(40) Arning, M. D.; Minteer, S. D. In *Handbook of Electrochemistry*; Zoski, C. G., Ed.; Elsevier: Amsterdam, 2007.
(41) Zhang, H.; Xu, J.-J.; Chen, H.-Y. *J. Phys. Chem. C* **2008**, *112*, 13886.
(42) Plowman, B.; Ippolito, S. J.; Bansal, V.; Sabri, Y. M.; O'Mullane, A. P.; Bhargava, S. K. *Chem. Commun.* **2009**, 5039.
(43) Zhang, X. G.; Li, X. H.; Li, H. L. *J. Colloid Interface Sci.* **2001**, *234*, 68.
(44) Ye, W.; Yan, J.; Ye, Q.; Zhou, F. *J. Phys. Chem. C* **2010**, *114*, 15617.
(45) Hohman, J. N.; Kim, M.; Wadsworth, G. A.; Bednar, H. R.; Jiang, J.; LeThai, M. A.; Weiss, P. S. *Nano Lett.* **2011**, *11*, 5104.
(46) Shafiei, M.; Motta, N.; Hoshyargar, F.; O'Mullanc, A. P. Development of New Gas Sensors Based on Oxidized Galinstan. Presented at IEEE Sensors 2015, Busan, South Korea, Nov 1−4, 2015.
(47) Hoshyargar, F.; Khan, H.; Kalantar-zadeh, K.; O'Mullane, A. P. *Chem. Commun.* **2015**, *51*, 14026.
(48) Wiley, B.; Sun, Y.; Mayers, B.; Xia, Y. *Chem. - Eur. J.* **2005**, *11*, 454.
(49) Mowry, S.; Ogren, P. J. *J. Chem. Educ.* **1999**, *76*, 970.
(50) Ray, C.; Dutta, S.; Sarkar, S.; Sahoo, R.; Roy, A.; Pal, T. *RSC Adv.* **2013**, *3*, 24313.

DOI: 10.1021/jacs.6b05957
J. Am. Chem. Soc. 2017, 139, 1464−1471